Phase Separation in $Al_xGa_{1-x}As$ Nanowhiskers Grown by the Solution−Liquid−Solid Mechanism

Paul D. Markowitz,[†] Michael P. Zach,[‡] Patrick C. Gibbons,[§] R. M. Penner,[‡] and William E. Buhro*,[†]

Contribution from the Departments of Chemistry and Physics, Washington University, St. Louis, Missouri 63130-4899, and Department of Chemistry, University of California, Irvine, Irvine, California 92679-2025

Received July 14, 2000. Revised Manuscript Received March 16, 2001

Abstract: Low-temperature growth of $Al_xGa_{1-x}As$ by the solution−liquid−solid mechanism affords nanowhiskers having two specific overall compositions: $x = 0.1$ and 0.8. Intermediate compositions ($0.1 < x < 0.8$) are inaccessible by the method employed. Examination of the nanowhiskers by transmission electron microscopy, photoluminescence spectroscopy, electron energy loss spectroscopy, and annealing studies indicates that they possess compositionally modulated nanostructures. The observed compositional modulation consists of alternating comparatively Al-rich and Ga-rich $Al_xGa_{1-x}As$ domains with dimensions of 3−20 nm. The spontaneous phase separation, which occurs during growth, appears to be kinetically driven, and the resulting phase-separated nanostructures appear to be, therefore, metastable rather than stable. Spontaneous phase separation in $Al_xGa_{1-x}As$, which strongly influences its photoemission behavior, is not well understood theoretically.

Introduction

Ternary III−V semiconductors such as $Al_xGa_{1-x}As$ adopt homogeneous-alloy, ordered, or phase-separated (compositionally modulated) structures.[1−3] In an homogeneous alloy of general formula $M_xM'_{1-x}E$, the metal atoms M and M′ randomly occupy the "cation" sites in the crystal lattice, giving a single-phase solid solution. In an ordered $M_xM'_{1-x}E$ compound the metal atoms M and M′ occupy crystallographically specific (ordered) "cation" sites in the crystal lattice, also giving a single phase.[1,2] In a phase-separated $M_xM'_{1-x}E$ material a heterostructure of two, alternating ternary phases of different composition forms.[2,3] One of the phases is richer in M and poorer in M′ than is the other; that is, the value of x for the two phases differs.

We now report the results of transmission electron microscopy (TEM), photoluminescence spectroscopy, electron energy loss spectroscopy (EELS), and annealing studies conducted on $Al_xGa_{1-x}As$ nanowhiskers grown by a low-temperature, solution-based method. These studies strongly suggest that the $Al_xGa_{1-x}As$ nanowhiskers possess phase-separated nanostructures, which are unusual for $Al_xGa_{1-x}As$[4−8] and are not predicted by the AlAs−GaAs pseudobinary phase diagram.[9] Phase-separated nanostructures are known to significantly enhance the photoemission behavior of ternary semiconductors.

The blue, $In_xGa_{1-x}N$-based LEDs and laser diodes provide excellent examples of such photoemission enhancement.[10] These devices are grown on GaN films deposited on sapphire. The poor lattice match between GaN and the sapphire substrate induces formation of threading dislocations at densities sufficiently high to deactivate a conventional semiconductor light-emitting device.[10] Highly efficient emission from the $In_xGa_{1-x}N$ devices results from a spontaneous phase separation in the $In_xGa_{1-x}N$ layers, which generates nanometer-sized, comparatively In-rich $In_xGa_{1-x}N$ islands embedded in a comparatively Ga-rich $In_xGa_{1-x}N$ matrix.[10−14] Injected carriers (holes, or electrons and holes) are collected and confined in the lower-band-gap, In-rich islands, preventing their longer excursions to threading dislocations where they would recombine nonradiatively.[10,14] Consequently, radiative recombination is enhanced by the phase separation, which in the case of $In_xGa_{1-x}N$ is thermodynamically driven by the miscibility gap in the InN−GaN pseudobinary phase diagram (Figure 1).[15] Significantly, only $In_xGa_{1-x}N$ active layers emit with high efficiency,[16] GaN

* Corresponding author. E-mail: buhro@wuchem.wustl.edu.
[†] Department of Chemistry, Washington University.
[‡] Department of Chemistry, University of California, Irvine.
[§] Department of Physics, Washington University.

(1) Zunger, A. *MRS Bulletin* **1997**, *22(7, July)*, 20−26.
(2) Zunger, A.; Mahajan, S. In *Handbook of Semiconductors*; Moss, T. S., Ed.; Elsevier: Amsterdam, 1994; Vol. 3, 1399.
(3) Millunchick, J. M.; Twesten, R. D.; Lee, S. R.; Follstaedt, D. M.; Jones, E. D.; Ahrenkiel, S. P.; Zhang, Y.; Cheong, H. M.; Mascarenhas, A. *MRS Bulletin* **1997**, *22(7, July)*, 38−43.
(4) Petroff, P. M.; Cho, A. Y.; Reinhart, F. K.; Gossard, A. C.; Wiegmann, W. *Phys. Rev. Lett.* **1982**, *48*, 170−173.
(5) Chin, A.; Hsieh, K. Y.; Lin, H. Y. *Appl. Phys. Lett.* **1994**, *65*, 1921−1923.
(6) Chin, A.; Lin, B. C.; Gu, G. L.; Hsieh, K. Y. *Appl. Phys. Lett.* **1995**, *67*, 3617−3619.
(7) Hsieh, K. C.; Hsieh, K. Y.; Hwang, Y. L.; Zhang, T.; Kolbas, R. M. *Appl. Phys. Lett.* **1996**, *68*, 1790−1792.
(8) Chin, A.; Lin, B. C.; Gu, G. L.; Hsieh, K. Y. *J. Appl. Phys.* **1996**, *79*, 8669−8674.
(9) Wei, S.-H.; Ferreira, L. G.; Zunger, A. *Phys. Rev. B*, **1990**, *41*, 8240−8269.
(10) Nakamura, S. *Science* **1998**, *281*, 956−961.
(11) Narukawa, Y.; Kawakami, Y.; Funato, M.; Fujita, S.; Fujita, S.; Nakamura, S. *Appl. Phys. Lett.* **1997**, *70*, 981−983.
(12) Chichibu, S.; Wada, K.; Nakamura, S. *Appl. Phys. Lett.* **1997**, *71*, 2346−2348.
(13) McCluskey, M. D.; Romano, L. T.; Krusor, B. S.; Bour, D. P.; Brennan, S. *Appl. Phys. Lett.* **1998**, *72*, 1730−1732.
(14) Chichibu, S. F.; Marchand, H.; Minsky, M. S.; Keller, S.; Fini, P. T.; Ibbetson, J. P.; Fleischer, S. B.; Speck, J. S.; Bowers, J. E.; Hu, E.; Mishra, U. K.; DenBaars, S. P.; Deguchi, T.; Sota, T.; Nakamura, S. *Appl. Phys. Lett.* **1999**, *74*, 1460−1462.
(15) Ho, I.-H.; Stringfellow, G. B. *Appl. Phys. Lett.* **1996**, *69*, 2701−2703.

10.1021/ja0025907 CCC: $20.00 © 2001 American Chemical Society
Published on Web 04/18/2001

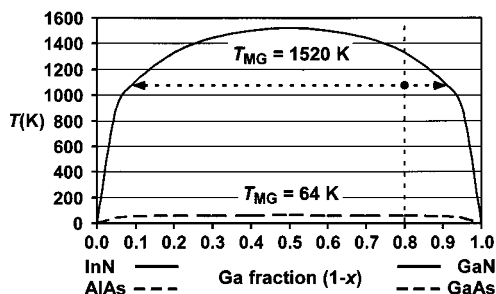

Figure 1. Pseudobinary InN−GaN[15] and AlAs−GaAs[9] phase diagrams showing the miscibility gaps present in each system. The given T_{MG} values are the upper consolute temperatures for closure of the miscibility gaps. The dotted lines and point portray a representative growth temperature and overall composition for $In_xGa_{1-x}N$ incorporated into LEDs and laser diodes.[10] Because the point lies within the miscibility gap, a phase separation is thermodynamically favored. The arrowheads identify the expected compositions of the two phase-separated constituents.

active layers do not, because only $In_xGa_{1-x}N$ is prone to a spontaneous phase separation during growth.[10]

In contrast, the thermodynamic miscibility gap in the AlAs−GaAs pseudobinary phase diagram is depressed to very low temperature (T_{MG} = 64 K),[9] and thus conventionally grown $Al_xGa_{1-x}As$ materials are homogeneous alloys (see Figure 1). However, spontaneous phase separation in $Al_xGa_{1-x}As$ has been observed in films deposited by low-temperature molecular beam epitaxy (MBE) upon specific substrates and substrate orientations.[4−8] These films possess lamellar, compositionally modulated nanostructures. The origin of the phase separation has been ascribed to various kinetic and thermodynamic effects operating at the surface or immediate subsurface of the growing films,[1,3,4,7,17−26] but remains incompletely understood.[3,27] Significantly, the lamellar, phase-separated $Al_xGa_{1-x}As$ films exhibit photoluminescence intensities of up to 3 orders of magnitude higher than those of the corresponding homogeneous-alloy films.[8] As in the $In_xGa_{1-x}N$ examples, collection and confinement of carriers in the lower-band-gap regions, in these cases the comparatively Ga-rich layers, enhance radiative recombination.[5,6,8]

Spontaneous phase separation is therefore a potentially attractive means for optimizing the photoemission properties of semiconductor nanostructures. Phase separation is conceptually related to the construction of core−shell heterostructured quantum dots, by which photoemission has also been enhanced.[28−37] Characterizing phase-separated nanostructures having domain sizes in the range of ca. 3−20 nm in $Al_xGa_{1-x}As$ nanowhiskers was challenging and required us to collect and compare the results of several complementary microscopic and spectroscopic techniques. Those analyses are detailed here.

We are not yet able to establish if photoemission in these phase-separated nanowhiskers is indeed enhanced relative to that of homogeneous-alloy analogues, for reasons outlined herein. However, to our knowledge no previous examples of spontaneous phase separation in semiconductor nanowhiskers have been documented.[38] Our nanowhiskers were grown by the solution−liquid−solid (SLS) mechanism,[39,40] which differs from the MBE process that afforded the prior phase-separated $Al_xGa_{1-x}As$ films.[4−8] For example, SLS growth does not employ a templating, oriented substrate. Thus, our results will contribute to a developing understanding of the phase-separation phenomenon in $Al_xGa_{1-x}As$. Specifically, the results demonstrate that misfit strain between a substrate and growing ternary crystal is not required to initiate spontaneous phase separation.

Experimental Section

All ambient-pressure procedures were carried out under dry N_2 using standard inert-atmosphere techniques. The $Al_xGa_{1-x}As$ products were generally stored and handled under inert atmospheres. However, the products were exposed to air for minutes to hours—to insert samples into the TEM, or to obtain XRD patterns—without apparent decomposition.

Materials. Ga metal and Al powder were used as received from Strem. Hexane was distilled over sodium. Thiophenol was distilled over $CaSO_4$. 1,3-Diisopropylbenzene was shaken with concentrated sulfuric acid to remove thiophene impurities, washed with water, and distilled over CaH_2. AsH_3 gas was used as received from Matheson. *Caution: AsH_3 is highly toxic and must be handled in accordance with proper safety measures.*[41] *We used AsH_3 from a lecture bottle by bubbling small amounts through reaction solutions in a well-ventilated hood and by passing the effluent gas from the reaction solutions through aqueous sodium hypochlorite to destroy unreacted AsH_3.* The organometallic precursors t-Bu_3Ga[42] and t-Bu_3Al[43] were prepared according to the literature.

Preparation of the Eutectic Al−Ga Alloy. Aluminum metal (0.0275 g, 1.019 mmol) and gallium metal (3.303 g, 47.37 mmol) were combined in a quartz tube and sealed under vacuum. The tube was heated to 700 °C overnight and then cooled to room temperature. Liquid

(16) Mukai, T.; Morita, D.; Nakamura, S. *J. Cryst. Growth* **1998**, *189/190*, 778−781.
(17) Zur, A.; McGill, T. C. *J. Vac. Sci. Technol. B* **1985**, *B3*, 1055−1060.
(18) Ipatova, I. P.; Malyshkin, V. G.; Shchukin, V. A. *J. Appl. Phys.* **1993**, *74*, 7198−7210.
(19) Tersoff, J. *Phys. Rev. B* **1997**, *56*, R4394−R4397.
(20) Venezuela, P.; Tersoff, J. *Phys. Rev. B* **1998**, *58*, 10871−10874.
(21) Guyer, J. E.; Voorhees, P. W. *Phys. Rev. Lett.* **1995**, *74*, 4031−4034.
(22) Ipatova, I. P.; Malyshkin, V. G.; Marududin, A. A.; Shchukin, V. A.; Wallis, R. F. *Phys. Rev. B* **1998**, *57*, 12968−12993.
(23) Léonard, F.; Desai, R. C. *Phys. Rev. B* **1998**, *57*, 4805−4815.
(24) Léonard, F.; Desai, R. C. *Appl. Phys. Lett.* **1999**, *74*, 40−42.
(25) Glas, F. *Appl. Surf. Sci.* **1998**, *123/124*, 298−302.
(26) Venezuela, P.; Tersoff, J.; Floro, J. A.; Chason, E.; Follstaedt, D. M.; Liu, F.; Lagally, M. G. *Nature* **1999**, *397*, 678−681.
(27) Mattila, T.; Wang, L.-W.; Zunger, A. *Phys. Rev. B* **1998**, *59*, 15270−15284.
(28) Dabbousi, B. O.; Rodriguez-Viejo, J.; Mikulec, F. V.; Heine, J. R.; Mattoussi, H.; Ober, R.; Jensen, K. F.; Bawendi, M. G. *J. Phys. Chem. B* **1997**, *101*, 9463−9475.
(29) Schlamp, M. C.; Peng, X.; Alivisatos, A. P. *J. Appl. Phys.* **1997**, *82*, 5837−5842.
(30) Peng, X.; Schlamp, M. C.; Kadavanich, A. V.; Alivisatos, A. P. *J. Am. Chem. Soc.* **1997**, *119*, 7019−7029.
(31) Bruchez, M. Jr.; Moronne, M.; Gin, P.; Weiss, S.; Alivisatos, A. P. *Science* **1998**, *281*, 2013−2016.
(32) Chan, W. C. W.; Nie, S. *Science* **1998**, *281*, 2016−2018.
(33) Gorer, S.; Penner, R. M. *J. Phys. Chem. B* **1999**, *103*, 5750−5753.
(34) Mitchell, G. P.; Mirkin, C. A.; Letsinger, R. L. *J. Am. Chem. Soc.* **1999**, *121*, 8122−8123.
(35) Cao, Y.-W.; Banin, U. *Angew. Chem., Int. Ed.* **1999**, *38*, 3692−3694.
(36) Schreder, B.; Schmidt, T.; Ptatschek, V.; Winkler, U.; Materny, A.; Umbach, E.; Lerch, M.; Müller, G.; Kiefer, W.; Spanhel, L. *J. Phys. Chem. B* **2000**, *104*, 1677−1685.
(37) Harrison, M. T.; Kershaw, S. V.; Rogach, A. L.; Kornowski, A.; Eychmüller, A.; Weller, H. *Adv. Mater.* **2000**, *12*, 123−125.
(38) Duan, X.; Lieber, C. M. *Adv. Mater.* **2000**, *12*, 298−302.
(39) Trentler, T. J.; Hickman, K. M.; Goel, S. C.; Viano, A. M.; Gibbons, P. C.; Buhro, W. E. *Science* **1995**, *270*, 1791−1794.
(40) Trentler, T. J.; Goel, S. C.; Hickman, K. M.; Viano, A. M.; Chiang, M. Y.; Beatty, A. M.; Gibbons, P. C.; Buhro, W. E. *J. Am. Chem. Soc.* **1997**, *119*, 2172−2181.
(41) Braker, W.; Mossman, A. L. *Effects of Exposure to Toxic Gases: First Aid and Medical Treatment*; Matheson Gas Products: East Rutherford, NJ, 1970; pp 37−38, 86−96.
(42) Kovar, R. A.; Derr, H.; Brandau, D.; Callaway, J. O. *Inorg. Chem.* **1975**, *14*, 2809−2814.
(43) Lehmkuhl, H. *Liebigs Ann. Chem.* **1968**, *719*, 40−49.

metal alloy (3.264 g, 98% yield) was retrieved from the quartz tube. Calculated composition: 97.9 mol % Ga, 2.1 mol % Al.

Preparation of $Al_{0.1}Ga_{0.9}As$. Liquid Al−Ga eutectic alloy (0.149 g, 2.17 mmol) and aluminum powder (0.045 g, 1.67 mmol) were combined in 1,3-diisopropylbenzene (25 mL). Thiophenol (21.3 μL, 0. 21 mmol) was added, and the heterogeneous slurry was stirred and heated to reflux for 3 h under nitrogen. In a separate flask, *t*-Bu_3Ga (0.501 g, 2.08 mmol) was dissolved in 1,3-diisopropylbenzene (9 mL). Excess AsH_3 gas was bubbled through this solution via a syringe needle for 6 min (500 bubbles/min) while stirring. The AsH_3 in stoichiometric excess was then removed by bubbling the solution with nitrogen for 2 h while stirring. The solution was then added dropwise over 3 h to the initially prepared, refluxing Al−Ga slurry. Refluxing was continued for an additional 19 h, and the resulting mixture was cooled. The $Al_{0.1}Ga_{0.9}As$ and metal products were collected as a dark-brown powder by filtering over a medium-porosity frit. The product was washed with hexane (3 × 10 mL) and dried under vacuum to yield 0.421 g.

The yield of the $Al_xGa_{1-x}As$ product was calculated using the following assumptions. The metal alkyl, in this case *t*-Bu_3Ga, was considered to be the limiting reagent, and the theoretical yield in moles of $Al_xGa_{1-x}As$ was set equal to the number of moles of metal−alkyl precursor. The 0.1 molar equivalent of precursor Ga in excess of the $Al_{0.1}Ga_{0.9}As$ product stoichiometry was assumed to have been returned to the Al−Ga alloy. Similarly, 0.1 molar equivalent of Al was assumed to have been incorporated into the $Al_{0.1}Ga_{0.9}As$ from the Al−Ga alloy. The mass of the Al−Ga alloy remaining at the conclusion of the synthesis was calculated by accounting for the Ga added and the Al subtracted and by assuming that the Al−Ga alloy was collected in the product with 100% recovery. The mass yield of $Al_{0.1}Ga_{0.9}As$ was taken to be the difference between the total mass collected and that of remaining alloy: 0.218 g (75%).

Preparation of $Al_{0.8}Ga_{0.2}As$. This procedure was conducted similarly to that above. Liquid Al−Ga eutectic alloy (0.099 g, 1.44 mmol) and thiophenol (21.9 μL, 0.21 mmol) were combined in 1,3-diisopropylbenzene (25 mL). The resulting heterogeneous slurry was stirred and heated to reflux for 17 h under nitrogen. (In other trials this reflux period was varied from 2 to 17 h without perceptibly affecting the outcome.) *t*-Bu_3Al (0.423 g, 2.13 mmol) in 1,3-diisopropylbenzene (15 mL) was used in place of *t*-Bu_3Ga. AsH_3 gas was bubbled through the *t*-Bu_3Al solution for 8 min (500 bubbles/min), and the excess AsH_3 was then purged by bubbling with nitrogen for 2 h. The purged solution was added dropwise over 1.5 h to the initially prepared, refluxing Al−Ga slurry. Refluxing was continued for an additional 5 h, and the resulting mixture was cooled. The $Al_{0.8}Ga_{0.2}As$ and metal products were collected as a dark-brown powder by filtering over a medium-porosity frit. The product was washed with hexane (3 × 10 mL) and dried under vacuum to yield 0.236 g. The yield of the $Al_{0.8}Ga_{0.2}As$ product, calculated as described above for $Al_{0.1}Ga_{0.9}As$, was 0.155 g (66%).

Annealing Studies. $Al_xGa_{1-x}As$ samples were sealed in silica tubes evacuated to 10^{-3} Torr. The sample tubes (which were under static vacuum) were then inserted into a tube furnace that had been preheated to the desired annealing temperature. At the conclusion of the annealing period (42 min at 700 °C for $Al_{0.8}Ga_{0.2}As$, and 15 min at 700 °C for $Al_{0.1}Ga_{0.9}As$), the sample tubes were removed from the furnace and allowed to cool to room temperature in air.

Powder X-ray Diffraction. XRD patterns were obtained using a Rigaku Dmax A vertical powder diffractometer with Cu Kα radiation (λ = 1.541845 Å) and Materials Data Incorporated (MDI) automation and Jade software. The XRD powder samples (1.5 × 2 cm smear mounts) were prepared in an N_2-filled glovebox and in some cases coated with a thin film of polyvinyltoluene (PVT) to minimize air exposure. The PVT film was applied by dripping a toluene solution of PVT onto the prepared XRD slide, allowing the toluene to evaporate. Powder patterns were compared to reference patterns from the JCPDS files (AlAs, 17-0915; GaAs, 32-0389; Al, 04-0787). The MDI software, which implements a form of the Scherrer equation, was used to calculate the coherence lengths for several peaks in the collected range.

Transmission Electron Microscopy. A JEOL 2000 FX instrument operating at 200 kV was used to collect normal bright-field images with no objective aperture and selected-area electron diffraction patterns. Bright- and dark-field images of whiskers aligned along the [110] zone axis were also obtained using an aperture that allowed only one diffracted beam to form an image. Samples were generally prepared by suspending 2−10 mg of powder in 5−10 mL of dry pyridine by sonication. A few drops of the resulting suspensions were pipetted onto holey-carbon-coated Cu TEM grids in a nitrogen-filled glovebox and evaporated to dryness. The TEM samples were stored in closed vials under nitrogen until insertion into the microscope. Elemental analyses were conducted on samples in the microscope using a Noran Voyager II energy-dispersive X-ray spectrometer.

Photoluminescence Spectroscopy. Powdered samples were dispersed on a nonfluorescent glassy carbon surface. Luminescence spectra were acquired using 50-mW continuous-wave excitation from a frequency-doubled argon-ion laser at 257 nm. Laser light with p-polarization was incident on the sample at Brewster's angle (~60°) from surface normal. Emission was collected at normal incidence through a 20× Zeiss EpiPlan microscope objective, N.A. = 0.45. The light was then coupled with an f4 lens into an imaging spectrograph (Chromex 250IS equipped with 300 groove mm^{-1} holographic grating; 500 nm blaze), which dispersed it onto a liquid-nitrogen-cooled CCD (Princeton Instruments model LN/1024EUV) having 1024 × 256 pixels. Signal from the 256 pixels arrayed perpendicular to the long axis of the CCD was binned, producing a linear detector with 1024 channels. The pixel-wise resolution of this detector was 2.3 meV. The sample was contained in a cryostat cooled with a closed-cycle helium refrigerator that permitted the sample temperature to be maintained at 20 K. Collection times varied between 0.05 and 30 s. Spurious signals from cosmic rays and dead CCD pixels were manually removed from all spectra.

EELS Images were collected using a JEOL 2010 FX transmission electron microscope. Single-crystal whiskers were oriented along the [110] zone axis, and energy-filtered images were formed using a Gatan imaging filter. Al maps were constructed as follows. For each pixel, the jump ratio at the Al−$L_{II,III}$ edge (the ratio of intensity at energies above vs below the $L_{II,III}$ threshold energy) was measured. Spectral overlap between Al, Ga, and As precluded the use of other edges for Al or Ga, as well as the use of the higher-contrast background-subtraction method for constructing element maps.

Results

Synthesis. Crystalline $Al_xGa_{1-x}As$ nanowhiskers were produced by the SLS mechanism (see eqs 1 and 2), described elsewhere,[39,40,44] in which nanowhiskers or nanofibers grow from nanometer-sized molten-metallic droplets dispersed in solution and fed organometallic precursors. Figure 2 shows representative nanowhiskers obtained from eqs 1 and 2, to which are attached the Al_yGa_{1-y} droplets that promoted their growth. The Al_yGa_{1-y} alloys used in eqs 1 and 2 were pregenerated from Al−Ga mixtures as bulk materials, which became dispersed as nanometer-sized droplets in the reaction mixtures as a natural consequence of the reactions. No measures were taken to induce or control this dispersion process. Catalytic amounts of PhSH were added to assist alkane elimination.[39,40]

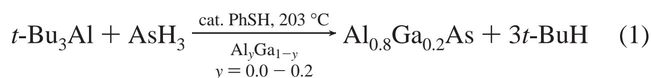

$$t\text{-}Bu_3Al + AsH_3 \xrightarrow[Al_yGa_{1-y},\ y = 0.0-0.2]{\text{cat. PhSH, 203 °C}} Al_{0.8}Ga_{0.2}As + 3t\text{-}BuH \quad (1)$$

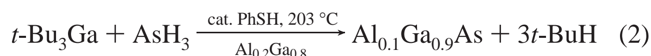

$$t\text{-}Bu_3Ga + AsH_3 \xrightarrow[Al_{0.2}Ga_{0.8}]{\text{cat. PhSH, 203 °C}} Al_{0.1}Ga_{0.9}As + 3t\text{-}BuH \quad (2)$$

In eqs 1 and 2, one metal in the $Al_xGa_{1-x}As$ products was incorporated chiefly or entirely from the organometallic precursor, and the other, from the Al_yGa_{1-y} alloy. Thus, the second metal was required in sufficient amounts in the initial metallic source. An initial composition corresponding to a molten alloy saturated in Al was required for eq 2 (which at the reaction temperature has composition $Al_{0.17}Ga_{0.83}$), whereas elemental

(44) Buhro, W. E.; Hickman, K. M.; Trentler, T. J. *Adv. Mater.* **1996**, *8*, 685−688.

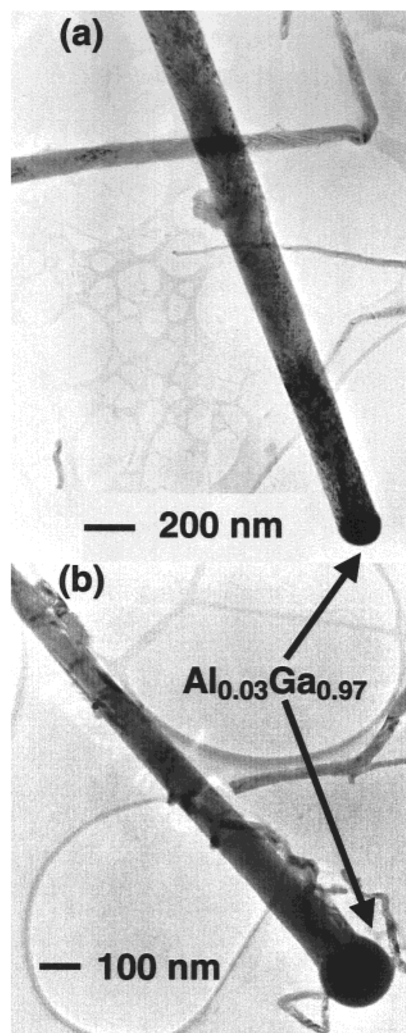

Figure 2. Representative $Al_xGa_{1-x}As$ nanowhiskers grown by the SLS mechanism. Note that representative metallic compositions of the attached alloy droplets are indicated. (a) An $Al_{0.8}Ga_{0.2}As$ nanowhisker from eq 1. (b) An $Al_{0.1}Ga_{0.9}As$ nanowhisker from eq 2.

Ga could be added as the initial metal source for eq 1. (Typically an Al−Ga eutectic was used as the initial metal source for eq 1, because it was experimentally more convenient than use of Ga.) Elemental Al could not be used in eq 2 because its melting point (660 °C) is too high, and therefore it does not disperse as metallic droplets under the reaction conditions.

The crystallinity and size distributions of the $Al_xGa_{1-x}As$ products were determined by XRD and TEM. XRD patterns of the bulk powders from eqs 1 and 2 possessed reflection widths consistent with crystalline coherence lengths of 30−60 nm. TEM images revealed mixtures of kinky polycrystalline fibers and near-single-crystal whiskers having diameters of ca. 20−200 nm (Figure 2). The lengths of these pseudo-1D structures were up to 8 μm. The images also contained small quantities of diffuse, fluffy structures, generally estimated at 10−20 vol % of the sample, which appeared to be amorphous $Al_xGa_{1-x}As$.

The nanowhiskers gave single-crystal electron-diffraction patterns (shown below) over regions several hundred nm in length, except near occasional stacking faults. The single-crystal regions were sometimes adjacent to polycrystalline regions within the same nanowhisker or nanofiber. Indexing of the single-crystal electron-diffraction patterns established that (111) close-packed crystal planes were oriented perpendicular to the nanowhisker long axes. That is, the nanowhiskers grew in the [111] direction of the $Al_xGa_{1-x}As$ zinc blende crystal structure.

The compositions of the nanowhiskers and nanofibers and attached alloy droplets were determined by energy-dispersive X-ray spectroscopy (EDS) in the TEM. Because of the close similarity of the AlAs and GaAs lattice parameters, the positions of the XRD reflections (in 2θ) for $Al_xGa_{1-x}As$ are only very weakly sensitive to x, and therefore the average bulk compositions of the products could not be determined from the XRD data. EDS data collected over 50-nm spot sizes gave $Al_{0.79\pm0.03}Ga_{0.21\pm0.03}As$ and $Al_{0.09\pm0.03}Ga_{0.91\pm0.03}As$ compositions for the products of eqs 1 and 2, respectively. These compositions were consistently uniform (within the error limits indicated) at various positions along the axial dimension of a nanowhisker or nanofiber, and in separate nanowhiskers or nanofibers within a sample. The compositional modulation we believe to be present in these nanowhiskers, discussed below, exists on a length scale shorter than can be detected by EDS. Representative compositions for the alloy droplets are indicated in Figure 2.

The absence of a thermodynamic miscibility gap in the AlAs−GaAs phase diagram (Figure 1) at the synthesis temperature (203 °C, 476 K) suggested that we should be able to grow $Al_xGa_{1-x}As$ nanowhiskers over the entire composition range $0.10 \le x \le 0.80$, the limiting compositions having been established by eqs 1 and 2. Consequently, eq 3 was undertaken using various mixtures of t-Bu_3Al and t-Bu_3Ga with the intent of producing $Al_xGa_{1-x}As$ nanowhiskers with intermediate compositions. The surprising results are summarized under eq 3. We were unable to produce nanowhiskers having *any* intermediate compositions. The products of these attempts were either crystallographically amorphous *or* were crystalline nanowhiskers having an identical composition to that established as the limiting case in eq 2.

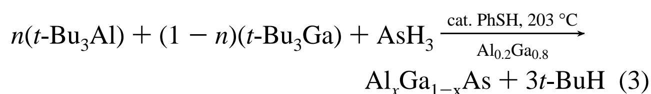

$$n(t\text{-}Bu_3Al) + (1-n)(t\text{-}Bu_3Ga) + AsH_3 \xrightarrow[Al_{0.2}Ga_{0.8}]{\text{cat. PhSH, 203 °C}} Al_xGa_{1-x}As + 3t\text{-}BuH \quad (3)$$

n	x	$Al_xGa_{1-x}As$ product structure
0.0	0.1 (eq 2)	crystalline nanowhiskers
0.2	0.1	crystalline nanowhiskers
0.3	−	amorphous
0.5	−	amorphous
0.8	−	amorphous/poorly crystalline
1.0	0.8 (eq 1)	crystalline nanowhiskers

The thermodynamic relationships expressed in Figure 1 cannot account for the observation of only two specific nanowhisker compositions resulting from the variety of synthetic conditions we investigated. As shown in eq 3 and discussed above, we examined a wide range of organometallic-precursor ratios. We also varied the initial metal−alloy compositions, the relative *amount* of the initial metal alloy, the period and sequence of organometallic-precursor addition, and the reflux period in eqs 1 and 2. The products resulting from these variations were either amorphous, or were nanowhiskers possessing one of the two compositions indicated in eqs 1 and 2. The results appear contrary to the reasonable extrapolation from Figure 1 that if any crystalline $Al_xGa_{1-x}As$ composition is kinetically accessible at the 476 K synthesis temperature, all should be accessible. In fact, the formation of only Al-rich or Ga-rich compositions could be consistent with the presence of an unexpected miscibility gap, if compositions within the gap are for some reason experimentally inaccessible. Interestingly, recent theoretical[23,24,45] and experimental studies[46] have identified "kinetic" miscibility gaps for ternary semiconductors, which

(45) González, D.; Aragón, G.; Araújo, D.; de Castro, M. J.; García, R. *Appl. Phys. Lett.* **1999**, *74*, 2649−2651.

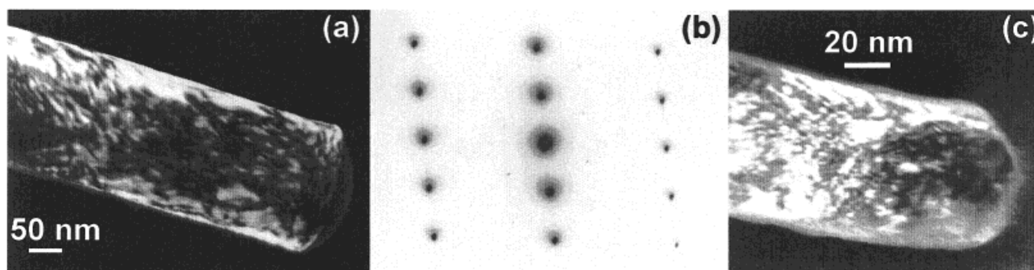

Figure 3. TEM data from $Al_{0.8}Ga_{0.2}As$ nanowhiskers. (a) A dark-field image formed from the composition-sensitive 200 diffracted beam of an unannealed nanowhisker. Note the strong light−dark pseudolamellar contrast. (b) An electron-diffraction pattern collected in a ⟨110⟩ zone from the nanowhisker in (a), establishing its single-crystal character. Indexing of the pattern establishes that the nanowhisker long axis is the [111] direction. (c) A dark-field image formed from the composition-sensitive 200 diffracted beam of a nanowhisker annealed at 700 °C for 42 min., showing that the light−dark image contrast is retained.

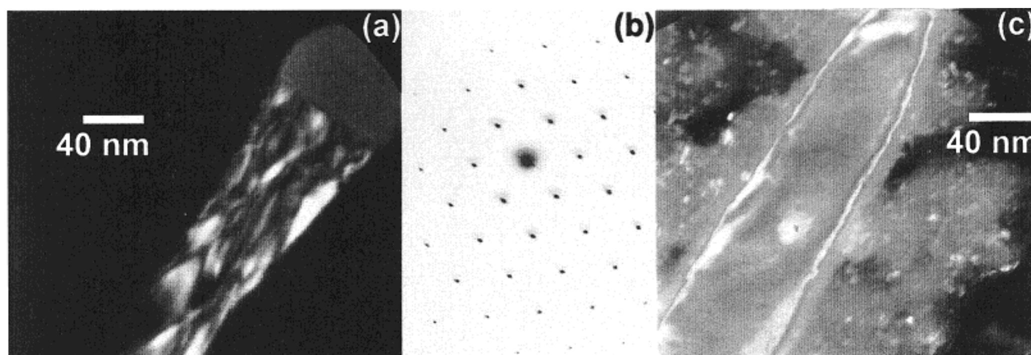

Figure 4. TEM data from $Al_{0.1}Ga_{0.9}As$ nanowhiskers. (a) A dark-field image formed from the composition-sensitive 200 diffracted beam of an unannealed nanowhisker. Note the strong light−dark pseudolamellar contrast. (b) An electron-diffraction pattern collected in a ⟨110⟩ zone from the nanowhisker in Figure 4a, establishing its single-crystal character. Indexing of the pattern establishes that the nanowhisker long axis is the [111] direction. (c) A dark-field image formed from the composition-sensitive 200 diffracted beam of a nanowhisker annealed at 700 °C for 15 min, showing that the strong light−dark image contrast is lost.

lie to higher temperature[45,46] than do the corresponding "thermodynamic" miscibility gaps (see the Discussion section). Alternatively, the growth of crystalline nanowhiskers possessing one of only two specific compositions and gross compositional uniformity could suggest existence of two local thermodynamic minima, of unknown origin, corresponding to the observed compositions.

Dark-Field TEM Imaging and Annealing Studies. Close inspection of normal, bright-field TEM images, like those in Figure 2, often revealed faint herringbone or pseudolamellar patterns in the $Al_xGa_{1-x}As$ nanowhiskers. This observation and the hint of an unexpected, "kinetic" miscibility gap suggested that the nanowhiskers might possess phase-separated nanostructures. As discussed earlier, spontaneous phase separation has produced lamellar, compositionally modulated nanostructures in certain $Al_xGa_{1-x}As$ films deposited by low-temperature MBE.[4−8] Consequently, we examined the nanowhiskers using the dark-field TEM-imaging method previously used to identify such compositional modulation (of x) in the $Al_xGa_{1-x}As$ films.[4−8]

Figure 3a shows a representative dark-field TEM image of an $Al_{0.8}Ga_{0.2}As$ nanowhisker, which contains a strong light−dark pseudolamellar pattern. The image was formed from the composition-sensitive 200 diffracted beam,[4] for which the light and dark regions would correspond to comparatively Al-rich and Al-poor regions, respectively,[4,7] if the pattern indeed resulted from a compositional modulation. However, such an image pattern could have other origins; specifically, the nanowhisker could be polycrystalline or possess an unaccompanied strain modulation; that is, one *not* accompanied by a composition modulation.[7] (Note that strain and composition modulations are often co-occurring and associated.[21,23−25]) Figure 3b shows a representative single-crystal electron-diffraction pattern collected over a 380-nm axial segment of the nanowhisker in Figure 3a, which ruled out polycrystallinity as the origin of the image pattern evident in Figure 3a.

To eliminate an unaccompanied strain modulation as the origin of the light−dark image pattern, the $Al_{0.8}Ga_{0.2}As$ sample from which Figure 3a,b was obtained was annealed under conditions (700 °C, 42 min) more extreme than those used previously to remove strain from the compositionally modulated, MBE-grown $Al_xGa_{1-x}As$ films (600 °C, 10 min).[7] The dark-field image in Figure 3c was collected from an annealed $Al_{0.8}Ga_{0.2}As$ nanowhisker. The strong light−dark image contrast was retained, suggesting that it was due to a compositional modulation having length scales of ca. 3−20 nm. Annealing at 1000 °C destroyed the $Al_{0.8}Ga_{0.2}As$ nanowhiskers.

Figure 4a shows a representative dark-field TEM image (formed from the 200 diffracted beam) of an $Al_{0.1}Ga_{0.9}As$ nanowhisker, the Ga-rich analogue to the nanowhiskers imaged in Figure 3. A strong light−dark image pattern was again evident. As above, this nanowhisker produced single-crystal electron-diffraction patterns over large areas (Figure 4b), ruling out polycrystallinity as the origin of the light−dark pattern. Annealing at 700 °C (15 min), however, removed the light−dark image texture from the $Al_{0.1}Ga_{0.9}As$ nanowhiskers, producing images that were fairly uniformly gray (Figure 4c). The gray, nearly featureless nanowhisker image in Figure 4c resembled the dark-field images (formed from the 200 diffracted beam) obtained from binary GaAs nanowhiskers[39] (not shown).

(46) González, D.; Aragón, G.; Araújo, D.; García, R. *Appl. Phys. Lett.* **2000**, *76*, 3236−3238.

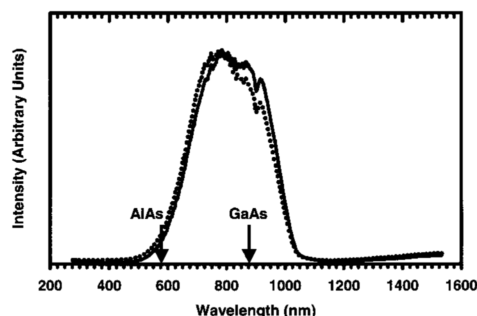

Figure 5. PL spectra recorded on unannealed (solid line) and annealed (dotted line; 700 °C, 42 min.) $Al_{0.8}Ga_{0.2}As$ nanowhiskers. The arrows indicate the expected emission wavelengths for binary AlAs and GaAs. The spectral intensities are arbitrarily scaled to be equal. The notches at 900 nm are instrumental artifacts.

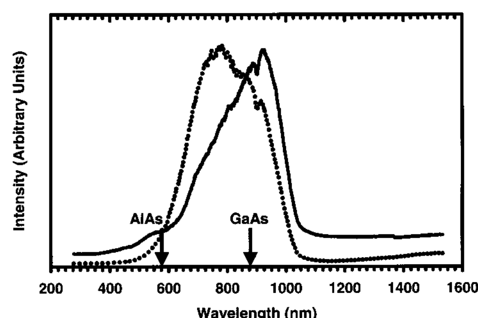

Figure 6. PL spectra recorded on unannealed (solid line) and annealed (dotted line; 700 °C, 15 min.) $Al_{0.1}Ga_{0.9}As$ nanowhiskers. The arrows indicate the expected emission wavelengths for binary AlAs and GaAs. The spectral intensities are arbitrarily scaled to be equal. The notches at 900 nm are instrumental artifacts.

Note that a compositional modulation of the type discussed here cannot be present in nanowhiskers of binary compounds such as GaAs.

The results of annealing the Ga-rich $Al_{0.1}Ga_{0.9}As$ nanowhiskers (Figure 4a vs 4c) could be attributed to relief of an unaccompanied strain modulation; that is, one might conclude that strain modulation alone was responsible for the light−dark pattern observed in the unannealed nanowhiskers (Figure 4a). Alternatively, the $Al_{0.1}Ga_{0.9}As$ annealing results could be attributed to relief of a composition modulation, in which an initial phase-separated nanostructure interdiffused upon annealing to afford a homogeneous alloy. We will ultimately establish that the latter conclusion is more consistent with the entire body of results presented here.

The light−dark image contrast in Figures 3 and 4a can be rationalized as composition modulations by the following arguments. If the light−dark patterns were due to strain modulation alone, then one would expect such patterns to exist also in binary GaAs nanowhiskers, which were grown by the same SLS mechanism under comparable conditions.[39] Instead, they were found only in the ternary nanowhiskers.

Additionally, phase-separated Al-rich and Ga-rich nanowhiskers *should* exhibit different annealing behavior. As a rule of thumb, $0.5T_M$ (where T_M is the absolute melting temperature) is often taken as the lower-limit recrystallization temperature of a bulk material.[44,47] The ternary phases $Al_{0.8}Ga_{0.2}As$ and $Al_{0.1}Ga_{0.9}As$ have solidus temperatures (T_S), akin to melting temperatures, of 1900 and 1520 K, respectively.[48] The approximate recrystallization temperatures $0.5T_S$ are then 680 and 490 °C, respectively. Only the latter is well below the annealing temperature employed (700 °C); consequently, interdiffusion of a phase-separated nanostructure should have been kinetically facile for $Al_{0.1}Ga_{0.9}As$ but much less so for $Al_{0.8}Ga_{0.2}As$. These rationalizations show that the dark-field imaging and annealing results are consistent with compositional modulations in the $Al_xGa_{1-x}As$ nanowhiskers. Further support for this viewpoint was obtained by photoluminescence spectroscopy.

Photoluminescence Studies. Figure 5 contains photoluminescence (PL) spectra collected from powder samples of unannealed and annealed $Al_{0.8}Ga_{0.2}As$ nanowhiskers, which indicated that emission occurred from phase-separated nanowhiskers. The emission features were broad, comparably so to those of porous silicon,[49,50] suggesting a distribution of emitting entities, possibly including quantum-confined emitting domains of various size, defect emitters, surface emitters, and emitting domains of various composition.[4] The emission envelope for the annealed sample was only very slightly shifted relative to that of the unannealed sample, consistent with the minimal change in nanostructure shown in Figure 3a versus 3c. The emission energy of $Al_xGa_{1-x}As$ is known to depend on x according to eq 4.[51] From eq 4 and the centers of the emission envelopes determined at half-height from Figure 5, which were 820 ± 5 and 800 ± 5 nm for the unannealed and annealed samples, respectively, we calculated the compositions of the average emitters to be $x_{\text{unannealed}} = 0.07 \pm 0.01$ and $x_{\text{annealed}} = 0.10 \pm 0.01$.[4] These calculations assume that the *centers* of the emission envelopes were more strongly influenced by composition than by any quantum-size effects, defect emitters, or surface emitters that may have been present.[4] The emitting compositions were therefore on average quite Ga rich, whereas the overall nanowhisker compositions were Al rich ($x = 0.8$), suggesting a compositional modulation of Al-rich and Ga-rich domains, with emission coming from the latter. Exclusive emission from the Ga-rich domains is expected because the electrons and holes generated upon excitation would preferentially recombine in the lower-band-gap domains, as was observed in the compositionally modulated $Al_xGa_{1-x}As$ films.[5−8]

$$E_g^{\Gamma}(\text{eV}) = 1.424 + 1.247x \quad (0 < x < 0.45) \tag{4}$$

Figure 6 contains PL spectra collected from powder samples of unannealed and annealed $Al_{0.1}Ga_{0.9}As$ nanowhiskers, which indicated that the emission occurred from phase-separated whiskers in the former case and homogeneous-alloy whiskers in the latter. Note that the emission envelopes of the unannealed and annealed $Al_{0.1}Ga_{0.9}As$ whiskers were significantly shifted with respect to one another (Figure 6), in correlation with the large change in nanostructure that occurred upon annealing, as revealed in Figure 4a versus 4c. As above, eq 4 and the half-height center of the emission envelopes were used to calculate the compositions of the average emitters. The half-height center wavelength of 867 ± 5 nm for the unannealed $Al_{0.1}Ga_{0.9}As$ whiskers yielded an average emitting $Al_xGa_{1-x}As$ composition of $x_{\text{unannealed}} = 0.005 \pm 0.008$, which is very close to binary GaAs. The half-height center wavelength of 800 ± 5 nm for the annealed $Al_{0.1}Ga_{0.9}As$ whiskers yielded an average emitting composition of $x_{\text{annealed}} = 0.10 \pm 0.01$, which is identical to the

(47) Dryburgh, P. M. *J. Cryst. Growth* **1988**, *87*, 397−407.
(48) Foster, L. M.; Scardefield, J. E.; Woods, J. F. *J. Electrochem. Soc.* **1972**, *119*, 765−766.
(49) Sailor, M. J.; Heinrich, J. L.; Lauerhaas, J. M. *Stud. Surf. Sci. Catal.* **1996**, *103*, 209−235.
(50) Gole, J. L.; DeVincentis, J. A.; Seals, L. *J. Phys. Chem. B* **1999**, *10*, 979−987.
(51) Casey, H. C., Jr. *J. Appl. Phys.* **1978**, *49*, 3684−3692.

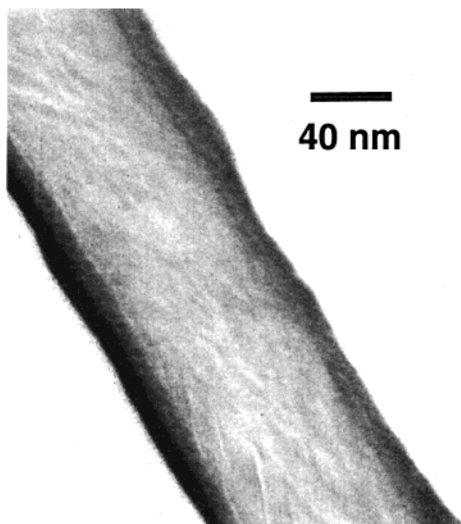

Figure 7. An Al map of a $Al_{0.8}Ga_{0.2}As$ nanowhisker obtained by EELS imaging.

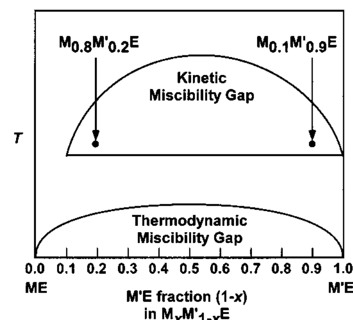

Figure 8. A proposed pseudobinary phase diagram for a general ternary semiconductor $M_xM'_{1-x}E$ that shows both thermodynamic and kinetic miscibility gaps (see text). The points refer to the two specific ternary compositions encountered in this study (see eqs 1 and 2).

overall composition of the nanowhiskers. The PL results strongly suggested that the unannealed nanowhiskers contained compositionally modulated nanostructures, for which emission occurred from Ga-rich (GaAs) domains, and further that this compositional modulation interdiffused upon annealing, as reflected in the TEM images (Figure 4a,c), such that emission then occurred from the "homogeneous" $Al_{0.1}Ga_{0.9}As$ alloy. The emission envelope for the annealed, $Al_{0.1}Ga_{0.9}As$−alloy nanowhiskers remained broad, presumably because the distribution of emitting entities proposed above was largely retained in the sample, including quantum-confined emitting domains of various size associated with the range of nanowhisker diameters in the sample, defect emitters, and surface emitters. Some of the emission breadth may also have been due to residual composition variations in the alloy structure.

EELS imaging. We sought a method capable of directly imaging the elemental fluctuations in the phase-separated $Al_xGa_{1-x}As$ nanowhiskers. Figure 7 shows an Al map of a $Al_{0.8}Ga_{0.2}As$ nanowhisker obtained by EELS imaging. Although the Figure-7 image *contrast* was fainter, the image *pattern* resembled the patterns observed for $Al_{0.8}Ga_{0.2}As$ nanowhiskers by dark-field TEM imaging (Figure 3a). The contrast mechanism in EELS imaging is different from that in dark-field TEM imaging, and so one does not expect to observe the same contrast in the two methods. Additionally, spectral interferences limited the contrast achievable in the Al map, and precluded construction of Ga maps entirely (see the Experimental section).

The faint patterns observed in Figure 7 are indeed most likely attributable to compositional modulations. Because EELS is not a diffraction-based imaging method, it is not sensitive to strain modulations, as dark-field TEM imaging is. Rather, the patterns in the EELS images could reflect thickness variations in the $Al_xGa_{1-x}As$ nanowhiskers. However, the edges of the nanowhiskers in the TEM images (Figures 3 and 4) appear to be smooth, ruling out significant thickness variations on the length-scale of the pattern features. Consequently, compositional modulation is the most likely origin of the patterns present in the EELS images.

Discussion

The evidence supporting compositional modulations in the $Al_xGa_{1-x}As$ nanowhiskers is summarized as follows. We find high-contrast light−dark patterns in dark-field TEM images directly comparable to those of phase-separated $Al_xGa_{1-x}As$ films, for which compositional modulation has been firmly established.[4−8] The form of dark-field imaging we have employed is considered the best primary evidence of such compositional modulation.[4−8] We have ruled out polycrystallinity as the origin of the observed dark-field patterns. That similar patterns are observed in EELS images casts doubt that they are caused by strain modulations *not* accompanied by compositional modulations. That the high-contrast light−dark patterns are absent from the dark-field images of binary GaAs nanowhiskers, capable of strain modulations but incapable of Al−Ga compositional modulations, also argues against unaccompanied strain modulations as the origin of the image patterns. The PL spectra of the proposed phase-separated $Al_xGa_{1-x}As$ nanowhiskers show the expected red-shifts caused by the compositional modulations.[5−8] From the PL data we have calculated average emitting compositions for the proposed phase-separated $Al_xGa_{1-x}As$ nanowhiskers that are significantly richer in Ga than are the overall nanowhisker compositions, as is required for compositionally modulated nanostructures. Finally, we have converted the proposed phase-separated $Al_{0.1}Ga_{0.9}As$ nanowhiskers to homogeneous-alloy nanowhiskers by annealing, and have observed the corresponding loss of the light−dark image patterns, and the corresponding blue shift in the PL spectrum that conforms to the homogeneous $Al_{0.1}Ga_{0.9}As$ composition. Therefore, although no single analysis or experiment irrefutably confirms the presence of compositional modulations in the $Al_xGa_{1-x}As$ nanowhiskers, the sum of the evidence is convincing.

As was alluded to earlier, the observation of compositional modulations may indicate the existence of an unexpected miscibility gap.[23,24,45,46] The recent literature describes two origins of immiscibility in binary or pseudobinary semiconductors, which are termed "thermodynamic" (conventional) and "kinetic" (unconventional),[22,23,45,46] and which produce miscibility gaps in different regions of the phase diagram as portrayed by the pseudobinary diagram in Figure 8.[45] One recent experimental study shows that in certain cases these miscibility gaps may even be separated from one another (rather than overlapping).[46] Outside of the miscibility gaps, crystal growth produces homogeneous-alloy structures. Inside the conventional, thermodynamic miscibility gap the single-phase homogeneous alloy is unstable and should phase separate into a compositionally modulated structure. Inside the "kinetic" miscibility gap, the single-phase homogeneous alloy is thermodynamically stable but kinetically inaccessible, such that a metastable phase separation occurs (see below). We surmise that our unexpected miscibility gap is a kinetic gap like that in Figure 8.

Our synthetic results may be rationalized according to Figure 8 as follows. The synthesis temperatures employed in eqs 1−3 (203 °C, 476 K) are substantially higher than the upper consolute temperature for closure of the thermodynamic miscibility gap (64 K),[9] as noted above, and so the compositional modulations observed in the $Al_xGa_{1-x}As$ nanowhiskers could not have been induced by this gap. However, the putative, higher-lying, kinetic miscibility gap would have induced the compositional modulations if the overall $Al_{0.1}Ga_{0.9}As$ and $Al_{0.8}Ga_{0.2}As$ compositions lie within it at the growth temperature (see Figure 8). This analysis does not account for our failure to produce $Al_xGa_{1-x}As$ nanowhiskers having intermediate compositions, which according to Figure 8 should also possess phase-separated nanostructures if $Al_{0.1}Ga_{0.9}As$ and $Al_{0.8}Ga_{0.2}As$ do. Presumably, other kinetic factors precluded crystal growth for compositions buried deep within the kinetic miscibility gap at the low growth temperature we employed. If grown within a kinetic miscibility gap as is suggested here, the phase-separated $Al_{0.1}Ga_{0.9}As$ and $Al_{0.8}Ga_{0.2}As$ nanostructures are metastable rather than stable, which is consistent with the annealing results for $Al_{0.1}Ga_{0.9}As$ nanowhiskers.

We now discuss the currently proposed origins of kinetic miscibility gaps in ternary semiconductors of general formula $M_xM'_{1-x}E$.[20−23,25,26,45] The literature analyzes kinetically induced compositional modulations in semiconductor films grown by MBE, chemical-vapor deposition, and liquid-phase epitaxy. In these cases, adspecies are deposited from a vapor or liquid nutrient phase onto the crystal-growth interface, which is the top surface of the growing film. The adspecies possess good diffusional mobility in the surface monolayer, because surface-diffusion rates are comparatively high. Certain effects operate in the surface monolayer, described below, that drive a phase separation (a spatial modulation of x) at the surface, the growth interface. As subsequent layers are deposited, the former surface layers become buried in the bulk of the film, and because bulk diffusion rates are comparatively very slow, the arrangements adopted while in the surface layer become frozen in the bulk. Thus, compositional modulation is transmitted to and retained in the bulk of the film, although it is not thermodynamically favored in the bulk. The fast diffusional kinetics at the surface coupled with the slow diffusional kinetics in the bulk lead to a growth-pathway-specific, metastable, phase-separated structure, and hence a “kinetic” miscibility gap.

Kinetic compositional modulations may be induced by misfit strain.[21,23,25] To our knowledge, all experimental examples of kinetically driven phase separation in semiconductors consist of films grown on substrates for which at least a small lattice mismatch or misfit exists. The misfit may be quantified by the parameter $\epsilon = (a_f - a_s)/a_s$, where a_f and a_s are the cubic lattice constants of the film and substrate, respectively.[21] The mismatch induces elastic misfit strain between the substrate and the initial overlayer of the growing film, which is accommodated by a spontaneous surface roughening of the overlayer. The hillock-and-valley structure produced by roughening allows the overlayer to remain crystallographically coherent with the substrate without introduction of misfit dislocations. As a result, a film (overlayer) grown on a substrate having a smaller lattice constant (positive ϵ) experiences a *compressive* strain, which is concentrated in the valleys, but is partially relaxed in the hillocks. In an overlayer grown with a negative ϵ, the *tensile* stress is concentrated in the valleys, but partially relaxed in the hillocks. In both cases, the stress in the overlayer is modulated by the hillock-and-valley structure.

In binary or pseudobinary overlayers, such as in a ternary semiconductor $M_xM'_{1-x}E$, surface roughening is always coupled with a spontaneous phase separation.[23] The binary or pseudobinary film has a composition-dependent lattice parameter a_f, which is determined by the relative amounts (e.g., x and $1 - x$) of the end-member components (e.g., ME and M′E) incorporated in various regions of the film. The dependence of a_f on composition is quantified by the solute expansion coefficient $\eta = (\Delta a_f/\Delta x)/a_f$.[21] In response to the stress modulation noted above, one end-member component (e.g., ME) becomes enriched in the hillocks, and the other (e.g., M′E), in the valleys.[20,21,24,26,52] For an overlayer grown under compression (positive ϵ) the end-member component of larger dimension is enriched in the hillocks, where the compressive stress is partially relaxed, and the end-member component of smaller dimension is enriched in the valleys, where the compressive stress is concentrated.[20,21,24,26,52] For an overlayer grown under tensile strain (negative ϵ) the opposite occurs: the larger component is enriched in the valleys and the smaller in the hillocks. Thus, an initial $M_xM'_{1-x}E$ overlayer deposited onto a misfit substrate acquires a spontaneous compositional modulation that is strongly correlated with the surface-roughening-derived stress field.

Several theoretical analyses show that the phase separation in the initial overlayer can become amplified in the subsequently deposited film.[20−23,25,26,45,52] The analyses use different detailed models and theoretical strategies, which are not described here. All evaluate various thermodynamic effects and kinetic processes that operate in the growth monolayer and influence compositional distributions. These influences may be distilled into two, one associated with surface thermodynamics and the other with surface kinetics.[52] (1) As noted above, a thermodynamic driving force exists at the surface of a compressively strained overlayer to incorporate the larger component into the hillocks and the smaller component into the valleys. Thus, as growth proceeds, the surface roughness tends to increase,[23,52] and so too does the surface driving force for phase separation. (2) The compositional modulation at the growth interface sets up a modulation in chemical potential.[22,26] The faster-diffusing component (e.g., M′E) competes most effectively for the incorporation sites of lowest chemical potential.[22,26,52] These two effects may work in concert and amplify the phase separation in the growing film until a saturation level is achieved.[22]

As noted above, the experimental examples of kinetically driven phase separation have occurred in films grown on substrates, where at a least a small substrate−film misfit was present[23,26] or presumed to be present.[20,25] But is a substrate−film misfit *required* to initiate a kinetically amplified phase separation? Several of the theoretical treatments allow compositional modulations to develop in the absence of misfit; that is, with $\epsilon = 0$.[22,23,26,45,52] One theoretical study states explicitly that under appropriate circumstances a kinetic phase separation may be initiated by the infinitesimal compositional fluctuations present in any alloy.[22] Other theoretical studies allow kinetic phase separation to proceed with $\epsilon = 0$, provided that the solute expansion coefficient η for the film is sufficiently large.[23,52] To our knowledge, we have observed kinetically driven phase separations in semiconductor crystallites grown *without a substrate* for the first time. Because there can be no misfit in the absence of a substrate, we assign an ϵ value of zero to our cases. Similarly, in the previously known phase-separated $Al_xGa_{1-x}As$ films grown on GaAs,[4−8] ϵ was exceedingly small ($\epsilon \leq 1 \times 10^{-3}$). These examples establish kinetic compositional

(52) Spencer, B. J.; Voorhees, P. W.; Tersoff, J. *Phys. Rev. Lett.* **2000**, *84*, 2449−2452.

modulations in the absence or near absence of misfit strain, which seems to confirm that infinitesimal compositional fluctuations alone[22] provide sufficient initiation.

In view of the preceding discussion, $Al_xGa_{1-x}As$ nanowhiskers are very *unlikely* candidates for a kinetically induced compositional modulation. The solute expansion coefficient for $Al_xGa_{1-x}As$ is exceedingly small, $\eta = 1 \times 10^{-3}$, because of the very similar lattice constants of AlAs ($a_{AlAs} = 5.662$ Å) and GaAs ($a_{GaAs} = 5.654$ Å). Surprisingly, we observe spontaneous phase separation where $\epsilon = 0$ and $\eta \approx 0$, whereas the tendency toward kinetic phase separation is predicted to increase with increasing absolute values of ϵ and η.[21,23,24,52] To illustrate the expected effect of $\eta \approx 0$, one would predict very little enrichment of AlAs in the hillocks and GaAs in the valleys in conjunction with the stress-relief mechanism described above, and hence a compositional modulation of vanishingly small amplitude. Stated dramatically, if one were to search for a case of kinetically driven compositional modulation without prior experimental knowledge, $Al_xGa_{1-x}As$ grown without a misfit strain is the last place one would look.

Because only some of the theoretical studies of kinetic compositional modulation are parametrized with ϵ and η,[21,23,24,52] we cannot easily compare and evaluate all of these studies in light of the surprising results with $Al_xGa_{1-x}As$ films[5−8] and nanowhiskers. Even so, phase separation in $Al_xGa_{1-x}As$ appears to be an ideal case to challenge and possibly distinguish the theoretical treatments and our fundamental understanding of the kinetic phase-separation phenomenon. Zunger has stated that atomic ordering in $Al_xGa_{1-x}As$ is still the least understood case of atomic ordering in pseudobinary semiconductors.[1] The present discussion emphasizes that kinetic phase separation in $Al_xGa_{1-x}As$ is the least understood case of phase separation in pseudobinary semiconductors.[20,25] Consequently, new theoretical studies that specifically address the $Al_xGa_{1-x}As$ case would be extremely valuable.

The preceding discussion has sought a structural, energetic, and mechanistic origin for kinetically induced compositional modulations in $Al_xGa_{1-x}As$ nanowhiskers. We must also consider if mere oscillations or fluctuations in experimental parameters may have been responsible. Striations attributed to fluctuations in alloy compositions or dopant levels in crystals grown from the melt have long been known.[53−60] In such cases, the compositional fluctuations (growth striations) are believed to arise from oscillating growth rates associated with temperature fluctuation. The temperature fluctuation is ascribed either to thermal convection in the melt, or to periodic movement—such as rotation—of the growing crystal through a temperature gradient.

Similarly, fluctuations of phosphorus-dopant levels have produced growth striations in silicon-whisker crystals grown by the vapor−liquid−solid (VLS) mechanism.[61] The VLS mechanism is directly analogous to the SLS mechanism employed here,[39] except that it operates under chemical-vapor-deposition conditions at higher temperatures. The compositional fluctuations in the VLS-grown whiskers are also ascribed to growth-rate oscillations.[61] Because our $Al_xGa_{1-x}As$ nanowhiskers grow while tumbling in a stirring, refluxing suspension, temperature oscillations that may have induced compositional fluctuations seem possible.

However, important distinctions exist between the growth striations produced by temperature oscillation, described above, and those found here in $Al_xGa_{1-x}As$ nanowhiskers. Growth striations arising from temperature oscillation consistently form as *planar* striations parallel to the growth interface,[53−56,61] and perpendicular to the growth direction, which we do not observe (see Figures 3 and 4). Furthermore, growth striations arising from temperature oscillation form on length scales that are three or more orders of magnitude *longer* than those of the compositional modulations in our $Al_xGa_{1-x}As$ nanowhiskers.[53−56,61] Finally, we have been unable to find prior reports of growth striations arising from temperature oscillation during growth of $Al_xGa_{1-x}As$ crystals. Therefore, although we cannot exclude temperature oscillation as the origin of the observed compositional modulations in $Al_xGa_{1-x}As$ nanowhiskers, our observations are not consistent with the existing experimental precedents.

We noted above a similarity between phase-separated nanowhiskers and core−shell nanocrystals, in which an emitting semiconductor core is confined within a shell of a larger band-gap semiconductor.[28−37] Core−shell nanocrystals exhibit enhanced emission quantum yields (of order 50%) and enhanced photostabilities relative to their single-component (core-only) analogues, because of more-effective carrier confinement and radiative recombination in the cores.[28,30,31] One may consider a phase-separated nanowhisker to consist of numerous core−shell structures bundled compactly together, and thus similar enhancements in photoemission properties may be anticipated. We have not yet been able to verify this expectation by comparing the emission quantum yields of phase-separated and homogeneous-alloy nanowhiskers because of our present inability to quantify sample emission. We collected our PL spectra from powders, for which reliable means to measure the sample volumes undergoing excitation are lacking. We are currently working to solubilize the nanowhiskers to allow PL spectra to be collected from solutions of known concentration, which would allow quantitative comparison of emission yields. Core−shell semiconductor nanocrystals are under investigation for use in hybrid organic−inorganic LEDs.[29,62] Phase-separated nanowhiskers may have similar potential applications.

Conclusions

Compositionally modulated $Al_xGa_{1-x}As$ nanowhiskers are grown by the low-temperature, substrate-free, solution−liquid−solid (SLS) mechanism. The observed phase-separated nanostructures do not result from bulk thermodynamic considerations. Rather, compositional modulation likely results from kinetic and perhaps (small or presently unidentified) thermodynamic effects operating at the crystal-growth interface between the nanowhisker and the attached, growth-promoting alloy droplet, which induce a kinetic miscibility gap. Spontaneous phase separation in this study occurs in the absence of misfit strain ($\epsilon = 0$) and in the case of an exceedingly small solute expansion coefficient

(53) Chase, A. B.; Wilcox, W. R. *J. Am. Ceram. Soc.* **1967**, *50*, 332−333.

(54) Warwick, C. A.; Brown, G. T.; Booker, G. R.; Cockayne, B. *J. Cryst. Growth* **1983**, *64*, 108−114.

(55) Wilcox, W. R. *J. Cryst. Growth* **1983**, *65*, 133−142.

(56) Rosenberger, F. *Fundamentals of Crystal Growth I*; Springer-Verlag: New York, 1979; pp 449−492.

(57) Müller, G.; Ostrogorsky, A. In *Handbook of Crystal Growth 2*, Part B; Hurle, D. T. J., Ed.; North-Holland: New York, 1994; pp 789−795.

(58) Vere, A. W. *Crystal Growth*; Plenum: New York, 1987; pp 38−40.

(59) Wilcox, W. R. In *Fractional Solidification*; Zief, M.; Wilcox, W. R., Eds.; Marcel Dekker: New York, 1967; Vol. 1, pp 166−167.

(60) Brice, J. C. *The Growth of Crystals from Liquids*; North-Holland: New York, 1973; pp 158−160.

(61) Wagner, R. S. In *Whisker Technology*; Levitt, A. P., Ed.; Wiley-Interscience: New York, 1970; pp 100−103.

(62) Mattoussi, H.; Radzilowski, L. H.; Dabbousi, B. O.; Thomas, E. L.; Bawendi, M. G.; Rubner, M. F. *J. Appl. Phys.* **1998**, *83*, 7965−7974.

($\eta = 1 \times 10^{-3}$), and is not well understood theoretically. The compositional modulations appear to be metastable, and appear to have developed from infinitesimal compositional fluctuations.

Acknowledgment. Funding was provided by NSF Grant CHE-9709104 (to W.E.B.) and NSF Grant DMR-9876479 (to R.M.P.). We gratefully acknowledge Dr. Alan Nichols, Electron-Microscopy Facility, Research Resources Center, University of Illinois at Chicago, for EELS imaging. W.E.B. thanks Dr. Alex Zunger (NREL) for helpful discussions. W.E.B. also thanks the anonymous reviewers for several important comments and suggestions.

JA0025907